A Fast Track Trigger with High Resolution for H1

H1 Collaboration

June 13, 1999

Abstract

To extend the triggering capabilities of the H1 experiment for exclusive final states involving tracks we propose to determine the momenta of charged particles measured in the central drift chamber with high precision in real time. Topological selection of final states will be made possible within 25 μs for the second level of the H1 trigger. Invariant mass calculations based on tracks such as $\Delta m = m_{K\pi\pi} - m_{K\pi}$ for the golden charm decay channel $D^* \rightarrow D^0\pi$ will be available after a few hundred μs for level 3. Altogether the *Fast Track Trigger* will supply the necessary factors of $\sim$100 reduction of trigger rates whilst maintaining high efficiency for track based signatures. Measurements such as beauty and charm cross sections will thus be made possible at a high luminosity HERA machine with high precision.

1 Introduction

For running beyond the year 2000 the ep collider HERA is planning a substantial increase of luminosity by insertion of focusing quadrupoles at the interaction points. A factor of approximately 5 increase over what is presently available will put new demands on triggering and event selection for the H1 experiment [1].

The H1 proportional chamber upgrade [2] will allow ep interactions to be selected at trigger level 1 (L1) with very high efficiency. If based on *track triggers* alone, this rate is dominated by photoproduction and low Q^2 processes[1], for which cross sections are large, leading to typical rates of a few hundred Hz. Exclusive final states of particular interest, such as those containing charmed mesons or vector mesons, constitute only a small fraction of this rate. Such final states can be distinguished from other ep interactions by reconstruction of either the relevant invariant masses from tracks in the central jet chamber (CJC) or by identifying a high momentum lepton. Specific software finders for these signatures are currently implemented on trigger level 4 (L4). It is assumed in the further discussion that the L4 selection capabilities will have been upgraded [3] to cope with the front-end analysis requirements, namely the larger fraction of exclusive processes relevant for physics.

With the advances in integration of modern electronics, drift chamber hit analysis can now be performed in real time without incurring any delay and trigger deadtime. This proposal therefore aims at an extension of the current readout system [4], leaving the original system fully operational. From a subset of wires in the drift chamber we will generate space coordinates from the hit analysis and subsequently perform a full momentum reconstruction in the remaining level 2 (L2) latency period of 25 μs. Information on the multiplicity and momentum of charged particles will thus be available to assist in the L2 decision. The final selection will be derived from invariant mass calculations for which several hundred μs are required, rendering them relevant for

[1] Q^2 is the absolute value of the four-momentum transfer squared at the electron vertex.

level 3 (L3) triggering. An example decay channel, representing the demanding requirements likely to be made on the system, is that of $D^* \rightarrow D\,\pi_s \rightarrow K\,\pi\,\pi_s$ which is selected by placing cuts on the values of $m_{K\pi}$ and $\Delta m = m_{K\pi\pi} - m_{K\pi}$.

The L2 and L3 triggers operate within the primary dead time of the readout and proceed before event building. The total reduction factor of order 100 over the total rate envisaged would be realised in a staged manner within this multi-level triggering scheme.

The proposed project requires novel implementations of hit finding, pattern recognition and mass reconstruction. Fast logic can be implemented in programmable digital devices at very large density. Modern tools for electronics design allow essential aspects of the project to be realised even with limited resources. It will yield significantly better selectivity than the existing DC$r\phi$ trigger [5] by reconstructing individual tracks in three dimensions with high resolution and down to much lower momenta.

In summary, we aim to introduce a fast partial readout of CJC 1 and 2, which will allow the further integration of triggering devices as described below, leaving the existing readout system untouched and available. Without such an upgrade of the trigger system essential parts of the physics programme will remain inaccessible at the high luminosity HERA machine.

2 Overview of Physics Rates

The HERA upgrade is targeted for a factor 5 increase in luminosity, with the goal of a peak luminosity of 70 μb^{-1}sec^{-1}. At these luminosities the basic physics rates for photoproduction events with a minimum requirement on the inelasticity parameter y and the rate of DIS at moderate Q^2 are large (see table 1 for some examples). At H1 the L4 input rate is limited to less than 100 Hz. To date events at all Q^2 can still be effectively triggered owing to a sophisticated strategy of prescaling [6], which essentially invokes the high rate physics triggers when luminosities have fallen sufficiently low in a given fill. However, the prescaling already now implies that a large fraction of events are unavailable for analysis.

Kinematical range	**Rate [Hz]**
Q^2 <1 GeV^2	1000
1< Q^2 <10 GeV^2	40
10 GeV^2< Q^2	4

Table 1: Approximate rates of the basic ep scattering process at peak luminosity of the upgrade HERA machine (0.05< y <0.95).

A large fraction of the luminosity increase will be achieved by increasing the proton and electron currents above present values (to 160 mA and 58 mA respectively). Hence we expect the beam induced non-ep backgrounds, which to first order scale with the current of the individual beam rather than their product, to increase by a smaller amount than the ep physics rate and the requirements on rates are mostly given by the increase in luminosities. However, backgrounds from sources such as synchrotron radiation from the electron beam are expected to increase by factors larger than the gain in luminosity because of the stronger focusing in the machine lattice.

3 Physics Motivation

By around 2005, it is expected that a total integrated luminosity of around 1 fb^{-1} will have been delivered by the upgraded HERA. Detailed information on the new physics topics that can be studied with such a large luminosity can be found in [7]. The implications for HERA and for the H1 experiment are discussed in [8]. This section introduces some of the physics analyses made possible by the upgrade for which an improved track trigger will be essential and demonstrates that the proposed device will meet the requirements. In section 3.1, measurements of low cross section processes relying on charged particle tracking are discussed. In section 3.2, the technical difficulties involved in triggering on such processes are explained. Section 3.3 contains a detailed study of the feasibility of selecting explicitly on open charm production at the early stages of the H1 trigger system. Section 3.4 summarises the triggering possibilities for a number of further processes and places the new device in context with existing trigger approaches after the upgrade.

3.1 HERA Physics with Charged Tracks Beyond the Upgrade

Using the large expected luminosities, it should be possible to make vastly improved measurements of many processes sensitive to the structure of the proton and photon and to the phenomenological consequences of quantum chromodynamics (QCD). Prominent among these processes are heavy flavour production and diffractive interactions. The accuracy of H1 measurements that have been made to date in both of these areas is limited most strongly by lack of statistics.

Measurements of open charm and beauty production are crucial to many aspects of the physics programme at HERA, as the heavy quark masses provide a natural cut-off preventing divergences in perturbative QCD calculations. Open charm data are sensitive to the gluon structure of the proton and photon, since the dominant production mechanisms are photon-gluon fusion $\gamma^{(*)}g \rightarrow c\bar{c}$ and (where the partonic structure of the photon is resolved) gluon-gluon fusion $gg \rightarrow c\bar{c}$. However, the cross sections for open heavy flavour production and branching ratios to detectable channels are small. Figure 1 shows H1 measurements of the gluon distribution of the proton using open charm data [9]. The statistical precision is presently no better than 25%. Less than three years' data from an upgraded HERA should be sufficient to measure the gluon density by this method to better than 10%. This would be a highly competitive measurement, giving greatly enhanced sensitivity to any differences between the gluon distribution as extracted from QCD fits to structure functions and from more direct measurements using open charm data.

After a few years of post-upgrade running, next-to-leading order QCD predicts that $\sim 10^8$ open charm events will have been produced in H1 [7]. With the enhanced detection capabilities afforded by the fully-commissioned central silicon detector, the total charm samples available will be sufficiently large to make investigations of $D^0\bar{D}^0$ mixing and searches for rare decays such as $D^0 \rightarrow \mu^+\mu^-$ [7]. Approximately 10^4 double charm tags could be collected by H1 with three years' data taking after the upgrade [7]. The distribution in the $c\bar{c}$ invariant mass would lead to a direct extraction of the proton gluon density. Studying correlations between the charmed and anti-charmed mesons in azimuth and p_t would provide further tests of QCD, charm production mechanisms and hadronisation models.

Through the study of charm production in diffractive events, the gluon content of the pomeron can be extracted. At present, only a few tens of events are available for analyses of this type [10]. First H1 measurements of open beauty production [11] have confirmed that cross sections are 1-2 orders of magnitude smaller than those for charm, but the measured rates are significantly larger than those predicted in the lowest order of QCD. Large increases in statistics are required to investigate these effects further.

Several other areas of H1 physics are presently compromised by low statistics. For example, 'elastic' vector meson production cross sections are more heavily suppressed with increasing Q^2 than is the case for the total

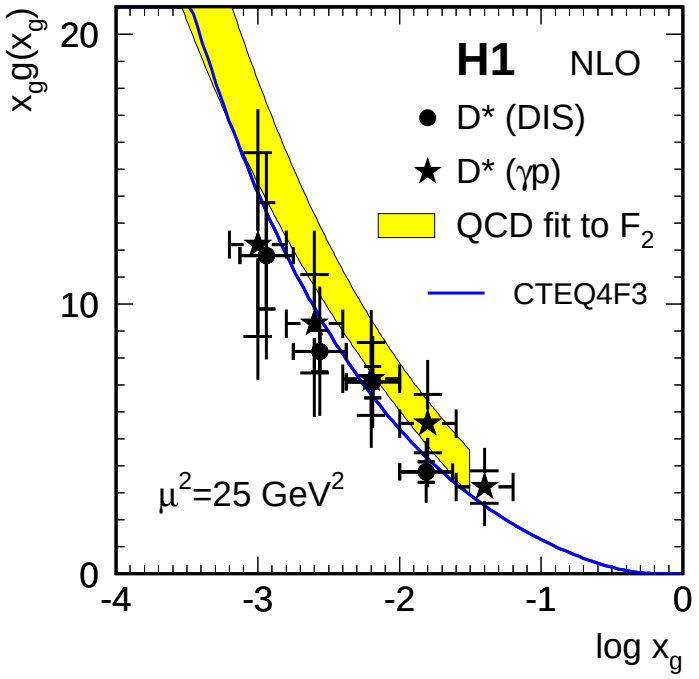

Figure 1: The gluon density of the proton at low x, as extracted using next to leading order QCD from D^* data in photoproduction ($Q^2 \approx 0$) and in DIS. The inner error bars are statistical. The outer error bars contain the statistical and systematic uncertainties added in quadrature. The data are compared to a measurement based on the scaling violations of $F_2(x, Q^2)$ and to a parameterisation based on global fits to a number of different measurements.

ep cross section. Precision measurements of the exclusive vector meson production processes $ep \to e\rho^0 p$ [12] and $ep \to eJ/\Psi p$ [13] have thus far been restricted to the region $Q^2 \lesssim 30$ GeV^2 and low[2] $|t|$. Measurements at larger Q^2 of the ratio of vector meson cross sections for longitudinal to transverse polarised photons, of the γp centre of mass energy and $|t|$ dependencies and of spin density matrix elements are crucial to our understanding of diffraction within QCD. The high $|t|$ region is believed to be a particularly good filter for hard diffractive processes in which the pomeron may be perturbatively calculable by considering the exchange of a pair of gluons from the proton, possibly evolving according to the BFKL equation [14]. To date, measurements in this region have relied on very poor statistics [15]. The observation of elastically produced Υ mesons has recently been reported by H1 [16]. Data samples based on orders of magnitude larger luminosities are required in order to test whether the $\gamma^{(*)}p$ centre of mass energy dependence of the process is stronger than that for elastic J/Ψ production, as is predicted by QCD inspired models based on the exchange of a pair of gluons from the proton [17]. Measurements of inelastic J/Ψ production are sensitive to the interplay between colour-singlet and colour-octet $c\bar{c}$ production mechanisms. Recent H1 measurements of inelastic J/Ψ production [13] are rather poorly described by the latest theoretical models. The larger statistics available from the upgraded HERA are essential to resolve the uncertainties in this field.

Final states that contain one or more very high p_t charged particle are almost always of interest. Inclusive charged particle spectra are sensitive to the dynamics of parton emission and hence to QCD evolution mechanisms. Charged particle spectra have been measured by H1 with good accuracy up to $p_t \sim 3$ GeV [18]. The higher p_t region, which can only be accessed with increased luminosity, is the most sensitive to the differences between the DGLAP and BFKL evolution schemes. High p_t charged particles are also produced in the leptonic decays of electroweak gauge bosons. Only a handful of W bosons have been identified by H1 to date. Many more will be produced with the luminosities available after the upgrade. The most significant anomalous signal in the present H1 data is the five events containing isolated high p_t muons in association with missing

[2] t is the four momentum transfer squared at the proton vertex.

transverse momentum [19]. The experimental selection for such events involves the requirement of a track with $p_t > 10$ GeV. It is clearly very important to search for further events with this signature after the upgrade.

3.2 The Need for Improved Triggering Methods

With the enhanced rates of ep interactions and backgrounds expected once HERA is upgraded, it will not be possible for H1 to continue to use the relatively open triggers currently employed, except in the case of very high Q^2 deep-inelastic scattering (DIS) events and other very high transverse momentum (p_t) processes. Many of the processes of interest for the study of proton / photon structure and QCD dynamics do not exhibit high p_t signatures. This is typically the case for the heavy flavour and vector meson production processes discussed in section 3.1. Without a dramatic improvement in the triggering capabilities of the experiment after the HERA upgrade, such events will be lost, or at best will be randomly prescaled such that only a small fraction are available for analysis. To retain such events with high efficiency, and thus to exploit the full physics potential of an upgraded HERA, on-line particle reconstruction in the early stages of the trigger is needed.

The event signatures for heavy flavour production are rather complicated. For example, open charm is usually identified through the decay channel $D^{*+} \rightarrow D^0\pi^+_{\rm slow} \rightarrow (K^-\pi^+)\pi^+_{\rm slow}$, by selecting on the intrinsically very narrow distribution in the mass difference $\Delta m = m(K^-\pi^+\pi^+_{\rm slow}) - m(K^-\pi^+)$. The D^* meson is usually produced with relatively low transverse momentum and the phase space available for this decay is small, such that the $\pi^+_{\rm slow}$ track has very small transverse momentum. We aim for a reconstruction threshold as low as 100 MeV.

To save vector meson events, it will be necessary to form invariant mass combinations of tracks from decays such as $\rho^0 \rightarrow \pi^+\pi^-$ and $J/\Psi \rightarrow \mu^+\mu^-$ / e^+e^-. To ensure that the vector meson is produced exclusively, information on the multiplicity of tracks will be required. To obtain samples of events at large $|t|$, it will be necessary to reconstruct the total transverse momentum of the vector meson decay products. To trigger on electroweak gauge boson decays and also to facilitate the measurement of inclusive charged particle spectra in the presence of a hard scale, it is necessary to identify high p_t tracks.

To identify open charm and high $|t|$, high Q^2 vector meson production on-line, the H1 trigger must therefore be able to identify efficiently tracks with a very low p_t threshold, to measure accurately their momenta and to determine the total track multiplicity. For the study of high p_t tracks, the p_t resolution of the trigger should remain good up to large p_t. Information on all three components of track momenta will be required in order to combine tracks to form Δm or vector meson invariant mass sums. Without a track trigger that meets these specifications, all analyses of processes that require the accurate combination of track measurements and do not contain high p_t final state particles will be seriously compromised.

3.3 Feasibility Study of the Triggering of Open Charm

The kinematics of charm production at HERA are such that the outgoing charm quarks are well contained in the central region of the H1 detector over a wide range in the fraction x_g of the proton momentum carried by the gluon entering the hard interaction. The main, alternative, direct method of extracting the gluon distribution of the proton is through dijet production, where the large $\gamma^{(*)}g$ invariant mass required to form the jet pair and to make it accessible for calorimetric detection implies that x_g must be relatively large. As illustrated by the pseudorapidity[3] (η) and p_t distributions in figure 2, D^* mesons arising from the process $\gamma^*g \rightarrow c\bar{c}$ are detectable in the central tracking detector ($|\eta| \lesssim 1.5$) with high efficiency for $10^{-3} < x_g < 10^{-1}$. Figure 2 also shows the η and p_t distributions of D^* mesons obtained from the process $\gamma^*g \rightarrow b\bar{b}$, where the b quarks decay to a c quark, which hadronises to produce a D^* meson. It is clear that the D^* mesons from b decays

[3]The $+z$ direction is taken to be the direction of the incident proton.

are produced more forward in the detector and with larger p_t than is the case for D^* mesons from direct c production, such that efficiencies are larger for beauty than for charm tagging.

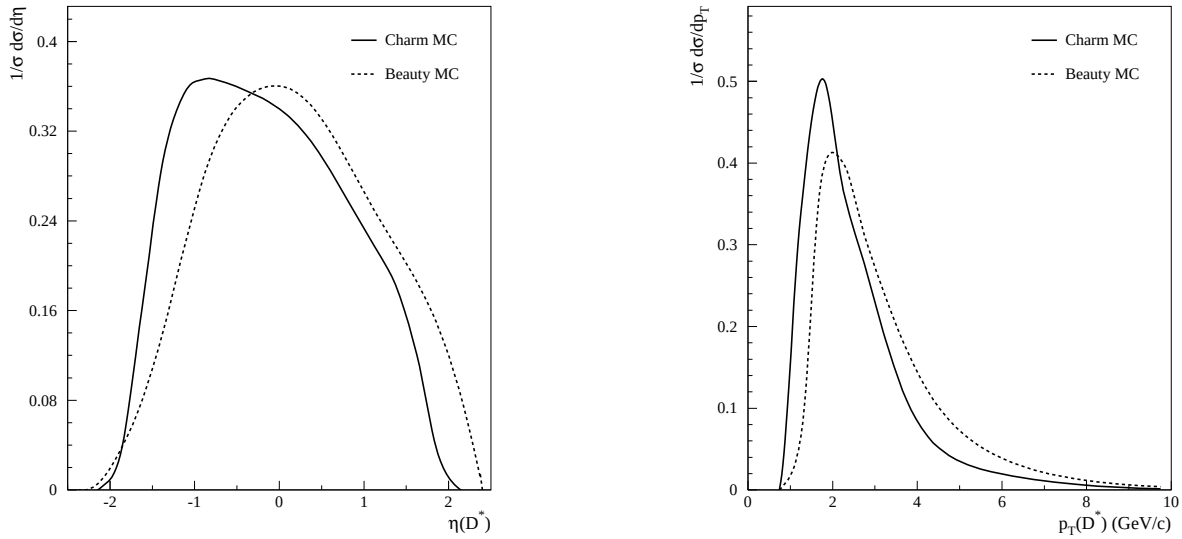

Figure 2: The η and p_t distributions of D^* mesons produced from $c\bar{c}$ and $b\bar{b}$ processes from AROMA [20] Monte Carlo simulations with $Q^2 > 1$ GeV^2 and $10^{-3} < x_g < 10^{-1}$. In both cases, the decay chain is $D^{*+} \rightarrow D^0\pi^+_{\rm slow} \rightarrow (K^-\pi^+)\pi^+_{\rm slow}$ and the requirements $p_t(K,\pi) > 300$ MeV, $p_t(\pi_{\rm slow}) > 120$ MeV are made.

In order to quantify the efficiencies, resolutions and background rejection power of the proposed Fast Track Trigger (FTT), we have simulated the performance of the device detailed in section 4 using measured hits of ep events.

It is usual to select D^* candidates by first combining tracks to form the invariant mass sum $m(K\pi)$. Where a pair of tracks yield a value of $m(K\pi)$ that is close to the nominal D^0 meson mass (within 80 MeV in typical off-line analysis), the $K\pi$ candidate pair are sequentially combined with all further tracks to form the D^* invariant mass $m(K\pi\pi_{\rm slow})$. The final selection is performed on the well resolved mass difference $\Delta m = m(K\pi\pi_{\rm slow}) - m(K\pi)$.

At the level 2 stage it will be possible to select events on the basis of track multiplicity and transverse momentum. For the D^* case, the requirement of three tracks, of which at least one positive and one negative track correspond to p_t >0.25 GeV, could be applied. Together with the identification of a scattered electron of 7 GeV or more, these requirements would remove approximately 80% of the DIS candidates without compromising the D^* selection efficiency.

Figure 3 shows the Δm distribution of a sample of DIS D^* candidates obtained by H1 in 1997 with the selection $p_t(D^*) > 1.5$ GeV, $p_t(K,\pi) > 0.3$ GeV and $p_t(\pi_{\rm slow}) > 0.12$ GeV. The Δm distribution is shown as reconstructed using off-line analysis tools and also as reconstructed according to the simulation of the track trigger. The resolution from the track trigger is sufficiently good for the majority of events to be found in the region of low Δm. Similar studies of the D^0 mass reconstructed by the track trigger reveal a resolution between 100 and 150 MeV. Cuts on the reconstructed $m(K\pi)$ and Δm are highly effective in the removal of background processes not containing D^* mesons and will form the basis of the Fast Track Trigger D^* identification at level 3.

To quantify the expected performance of the track trigger further, estimated efficiencies are determined by feeding the sample of DIS D^* candidates through the simulation and making various cuts on $m(D^0)$ and Δm as reconstructed by the track trigger. To estimate the expected output rates from the trigger with the same selection

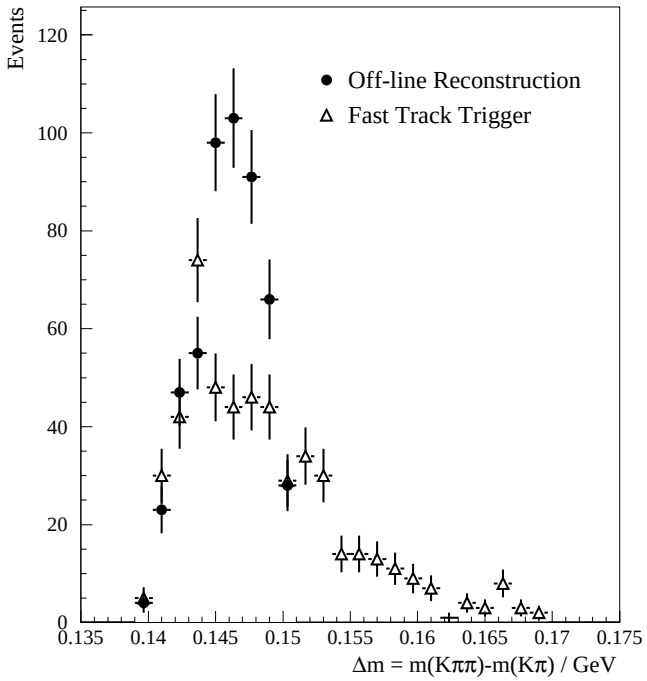

Figure 3: Illustration of the expected $\Delta m = m(K\pi\pi_{\rm slow}) - m(K\pi)$ resolution of the proposed trigger. The solid circles show the Δm distribution of a sample of D^* candidates from DIS events collected by H1 in 1997, as reconstructed using the best available off-line analysis tools ($|m(K\pi) - m(D^0)|$ <0.08 GeV, Δm <0.15 GeV). The open triangles show the Δm distribution for the same sample of events with tracks reconstructed using the simulation of the proposed track trigger.

criteria, a relatively unbiased sample of events triggered on the basis of a electron in the rear calorimeter (SpaCal) and a track requirement are also fed through the simulation. The number of events selected is used to determine the predicted trigger rate at the peak luminosity expected after the HERA upgrade of $70\ \mu{\rm b}^{-1}{\rm s}^{-1}$. In both cases, the requirements $p_t(D^*) > 1.5$ GeV, $p_t(K,\pi) > 0.3$ GeV and $p_t(\pi_{\rm slow}) > 0.12$ GeV are made in the track trigger selection. The results from both studies are shown in figure 4. Even with the proposed peak post upgrade luminosity, L3 output rates of less than 10 Hz are achievable whilst retaining 80% of events that would normally be analysed off-line. This can be achieved for example with cuts of $|m(K\pi) - m(D^0)|$ <300 MeV and $\Delta m < 160$ MeV. It should be noted that even once HERA reaches its design performance, the peak luminosity will be available only at the very beginning of a machine fill, when beam currents are largest. Average luminosities for the fully upgraded HERA will typically be half as large as the peak luminosities, with anticipated trigger rates smaller by a similar factor.

3.4 Rates and Efficiencies of the Trigger

The example of section 3.3 presents a technically demanding application for a charged track trigger. However, by no means does it exhaust the list of applications for such a device for which a few other examples are given below. Table 2 summarises some typical rates at the various levels. The "visible" cross sections include all branching ratios into the observed final state and the kinematical acceptance, e.g. the cuts of figure 3 for the DIS case. However, it should be noted that the L1 Keep rates are largely uncertain: they depend on the actual "coincidences" implemented to tackle the unknown beam backgrounds. They are correct in the sense that even

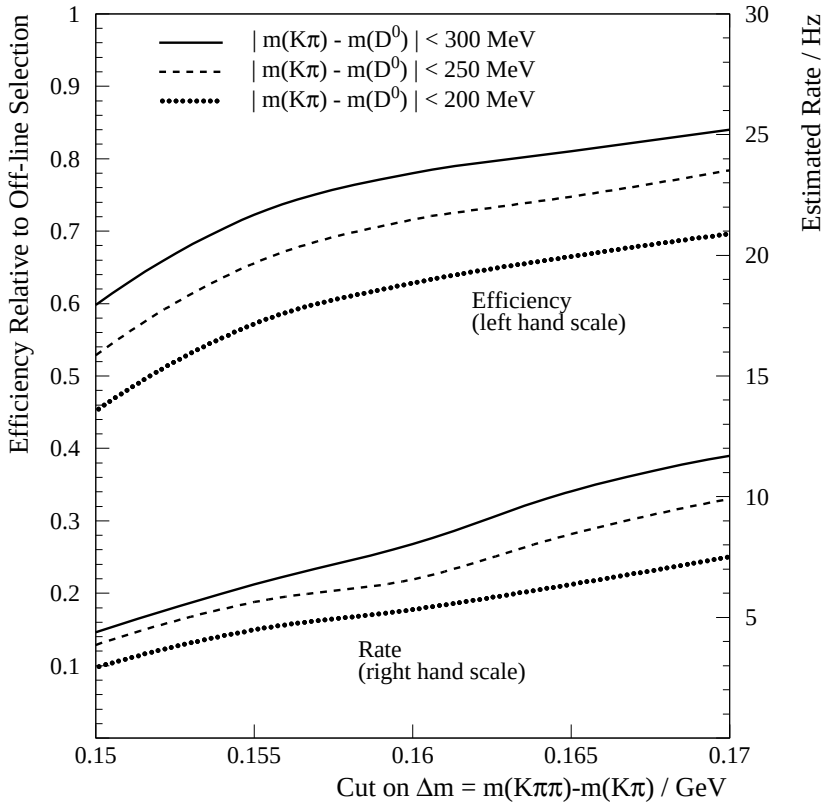

Figure 4: Estimated efficiencies and trigger rates for D^* mesons in DIS using the proposed trigger for various choices of cuts on the reconstructed D^0 mass and Δm. The efficiencies are relative to the off-line event selection used in the most recent H1 publication [9] and are calculated using a sample of DIS events collected in 1997. The expected rates are estimated using a sample of events collected using a SpaCal electron trigger and are extrapolated to the peak luminosity of $7 \times 10^{31}\ \mathrm{cm}^{-2}\mathrm{s}^{-1}$ that the upgraded HERA is expected to deliver.

today rates of several hundred Hz are common for triggers based on tracks alone and thus should be considered as reasonable examples. The efficiencies for triggering without FTT have been derived under the assumption of using a prescaled level 1 trigger such that the L2 Keep rate for that trigger remains at 1 Hz, which is very large and not tolerable for an extended number of such trigger channels.

	trigger rates with FTT [Hz]			visible cross section	trigger efficiency [%]	
Process	**L1**	**L2**	**L3**	$\sigma_{\rm vis}$ [pb]	with FTT	without
D^* decay (DIS)	500	100	5-10	150	50-80	1
D^* decay (γ p)	500	100	5-10	100	40-65	1
$\rho \to \pi^+\pi^-$ (DIS)	40	2.5	1	5000	80	2
J/$\Psi \to \mu\mu$,(ee)	50	20	1-3	1000	60(12)	3(1)
$\Upsilon \to \mu\mu$,(ee)	50	5	0.5-2	1.5	60(12)	3(1)
W $\to \mu\nu$	20	1	0.3	0.1	70	3

Table 2: Estimate of trigger rates and their reduction at the three different levels with and without the help of the Fast Track Trigger. The total visible cross sections and the expected trigger efficiencies normalised to the visible cross section is also shown. The rates are tentative and scaled to the expected peak luminosity of 70 μb^{-1}sec^{-1} using the L2 and L3 conditions as described in the text. The trigger rates for vector mesons differ for inelastic and elastic production because of the varying effectiveness of the track multiplicity requirement.

3.4.1 Vector Mesons

ρ: The decay particles of a ρ^0 have typical transverse momenta below the current threshold of the DC$r\phi$ trigger [5]. A level 1 trigger condition relying solely on good activity in the z-vertex trigger followed by a multiplicity requirement of exactly two reconstructed tracks from the Fast Track Trigger on level 2 would provide the necessary shield against the overwhelming background from, e.g., beam gas events. These requirements would also decrease the rates from ep interactions by 1-2 orders of magnitude, whilst retaining in excess of 80% of visible exclusive ρ candidates. For very low Q^2 physics such requirements would be implemented for short dedicated runs. For the deep-inelastically produced ρ the scattered electron provides an additional means of reduction.

J/Ψ: The two prong decays of the J/Ψ typically result in two back to back tracks of up to 1.5 GeV transverse momentum, for which again the background is large if momentum or mass selectivity is not available. For elastically produced J/Ψ, the total track multiplicity can again be restricted to 2 at the L2 stage of the trigger. For inelastically produced J/Ψ, an L2 cut on the highest p_t track in the event can be used to provide large reductions (see section 3.4.2). With an additional cut of $\pm$0.5 GeV around the nominal J/Ψ mass at the L3 stage, overall rate reduction factors of 50 are possible.

others: The Fast Track Trigger can be used at level 3 to search for several other vector meson states. Many of these have relatively low production cross sections and will therefore be interesting topics of study after the HERA upgrade. Further example channels are $\phi \to K^+K^-$, $\rho' \to \pi^+\pi^-\pi^+\pi^-$, $\Psi(2S) \to \ell^+\ell^-\pi^+\pi^-$ and $\Upsilon \to \ell^+\ell^-$, where $\ell^\pm$ denotes either $e^\pm$ or $\mu^\pm$.

3.4.2 High p_t Charged Particles

W (and Z) bosons are presently triggered by observing a lepton and an imbalance in the hadronic transverse recoil in the LAr calorimeter. This signature can only be reliably identified when the missing transverse momentum is large. Direct and prominent experimental signatures of the bosons are the produced μ and τ, which result in final states containing single particles at transverse momentum of many GeV. These particles will be recognised by the Fast Track Trigger and provide the extra distinction that allows the missing p_t calorimeter requirement to be relaxed [4]. Similarly, the signature of single charged particles of several GeV p_t, characteristic for the QCD processes mentioned in section 3.1 or for the hadronic decays of beauty mesons, can be detected at the trigger level.

Rate reduction factors of 10 and more are easily obtained with a high momentum requirement in the Fast Track Trigger as can be seen in figure 5 obtained from an unbiased sample of track triggered events. Both beam gas processes and γp with low invariant mass interactions produce their backgrounds predominantly in small transverse momentum particles.

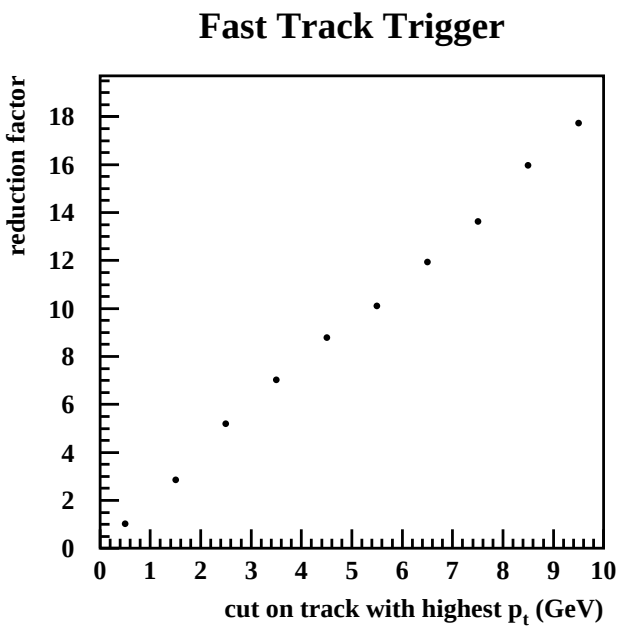

Figure 5: Rate reduction for a sample of track triggered events as a function of the requirement on the largest p_t track observed in the event.

3.5 Integration into the System of H1 Triggers

From the experimental point of view it has to be added that a Fast Track Trigger with flexible topological selectivity provides another safeguard against the uncertainties of the background conditions at the upgraded HERA. While this is difficult to quantify prior to startup, experience in the past has shown that, the larger is the flexibility for triggering, the better the experiment is able to cope with the sometimes demanding operation at a lepton hadron collider.

[4] The decay to electrons can be triggered with the calorimeter proper.

It also has to be added that the well defined momentum acceptance of the Fast Track Trigger will ease the understanding of trigger efficiencies in analyses. Overall, there will be only few essential hardware building blocks in setting up a physics trigger: z-vertex, calorimeters, tracks and muons. Three of these four components [2, 21] are undergoing upgrade programmes that effectively render such acceptance and efficiency studies more transparent.

Last but not least the track trigger can be combined with the improved calorimeter trigger at levels 2 and 3 to select special topologies consisting of single tracks and high energy jets, for which inelastic J/Ψ-production is just one example. We have not tried to expand on this list at this time but note that there is ample room for new dedicated triggers as the need arises.

4 Fast Track Trigger

Conceptually, the simplest way to select the physics channels discussed above is to trigger on events with minimum bias and then to analyse them in detail at L4. However, the maximum input rate to L4 is limited to less than 100 Hz (cf. table 1) for at least two reasons: firstly the present drift chamber readout requires a fast scanning of the memories of the fast analogue to digital converters (FADC) which takes up to 800 μs per event and secondly the sample and hold circuits of the calorimeter are multiplexed onto a few ADCs followed by DSP analysis which again takes some 800 μs in total.

We have considered an upgrade of the entire H1 online DAQ system [22] with the aim of attaining 1 kHz input rate to L4. However, it rapidly becomes clear that cost would be prohibitive and the change would require expertise in many instances no longer available to the collaboration. Such an upgrade is therefore not a realistic target.

The remaining option is to upgrade only the components necessary to enhance the selection power of the primary trigger levels, of which there are three (L1-L3). While such programmes are in progress for the calorimeter [21], the selectivity for final states with charged particles and little activity in the calorimeter is poor. This is the target of this proposal of a Fast Track Trigger.

The H1 central jet chamber [1] (CJC) consists of two concentric, rotationally symmetric drift chambers with wire planes parallel to the beam axis and 30^0 inclined to the radial direction. The first, inner chamber (CJC 1) consists of 30 cells of 24 wires each while CJC 2 uses twice as many cells with 32 wires each (fig. 6). The readout and triggering scheme proposed here will be limited to selected radial layers of CJC 1 and the first radial layers of CJC 2, in order to reduce complexity and cost of the upgrade.

The logical distribution of the envisaged analysis load over the trigger stages is depicted in Figure 7, summarising the time structure and reconstruction tasks. A *KEEP* condition at an earlier level causes the next level to be invoked. In the following sections an overview of this scheme is given. A detailed discussion of the implementation is given in Section 5.

One of the key requirements for successful triggering on exclusive final states is to increase the track acceptance at low momentum threshold. The proposed upgrade will provide an effective momentum threshold of 0.1 GeV and a momentum resolution of typically 5%.

4.1 Level 1

The present drift chamber readout continuously digitises the wire signals with FADCs sampling at 100 MHz. The samples are stored in a buffer for later readout and hit analysis. In the proposed upgrade the sampled data will immediately be analysed to determine, for each hit on a wire, the charge integral at both wire ends and the

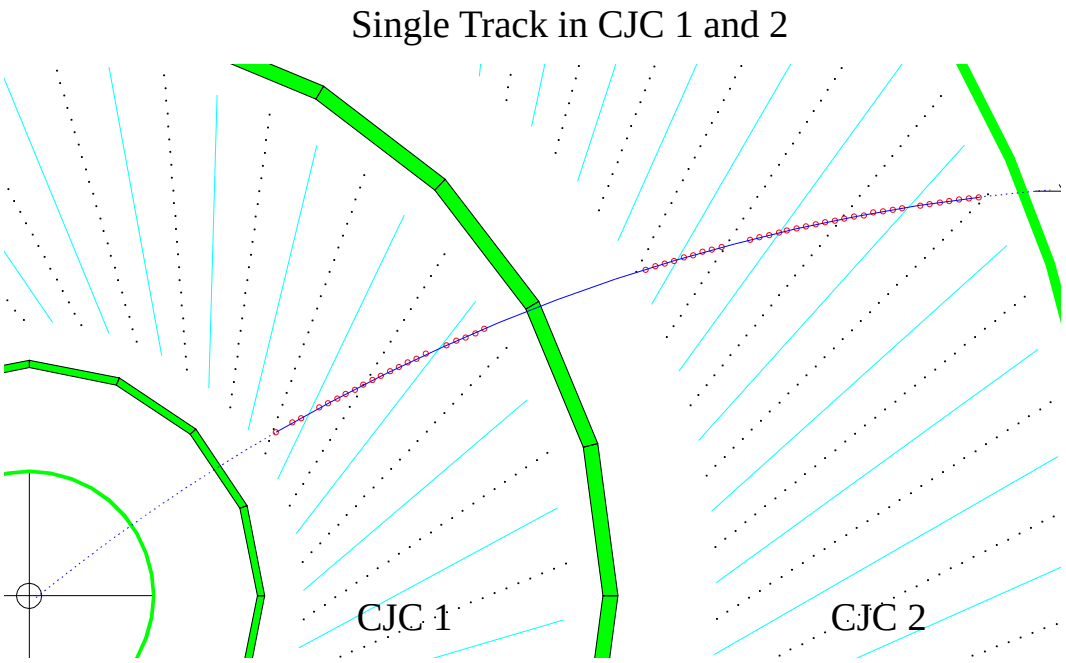

Figure 6: A partial cross section of the CJC 1 and 2 drift chambers and a reconstructed single track with the associated drift chamber hits. The position of the sense wires is indicated, as is the cathode plane between cells.

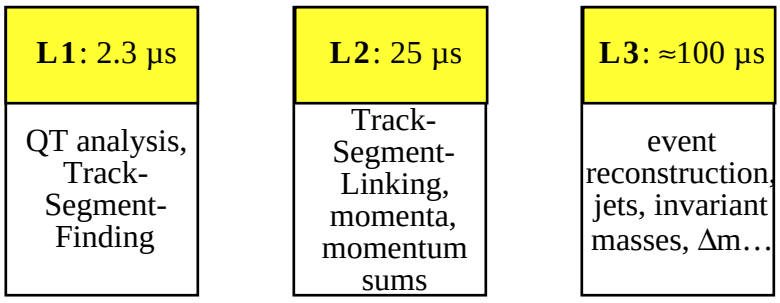

Figure 7: The allocation of the different reconstruction tasks to the various trigger levels. While the L1 and L2 decision times are fixed an L3 reject condition can be issued any time before the otherwise forced L3 Keep at 800 μs.

time of arrival. The procedure will be well contained within the L1 Keep latency of 2.3 μs, including drift time variations of up to 1 μs thus incurring no deadtime.

At the latest at L1 Keep the analysed hit data will be available for subsequent track finding. However, our goal is an approach, in which the track segment finding, which already provides initial momentum information, is placed into the L1 Keep latency. This option would allow the momentum acceptance to be reduced below the threshold of $\approx$450 MeV of the existing level 1 drift chamber track trigger. Since this increases the complexity of the level 1 trigger beyond a level that has been studied in sufficient detail, we do not elaborate this option any further for the time being.

The resulting momentum threshold for track segments is demonstrated in figure 8. Triplets of adjacent wires have been chosen at radii r between 24 and 59 cm, where the latter comprises the first radial layers of CJC 2. Tentatively, we have selected layers (2,4,6), (10,12,14) and (18,20,22) of CJC 1 and layers (4,6,8) of CJC2. The response for positive and negative tracks differs at large radii because of the less favourable track inclination with respect to the wire plane (fig. 6).

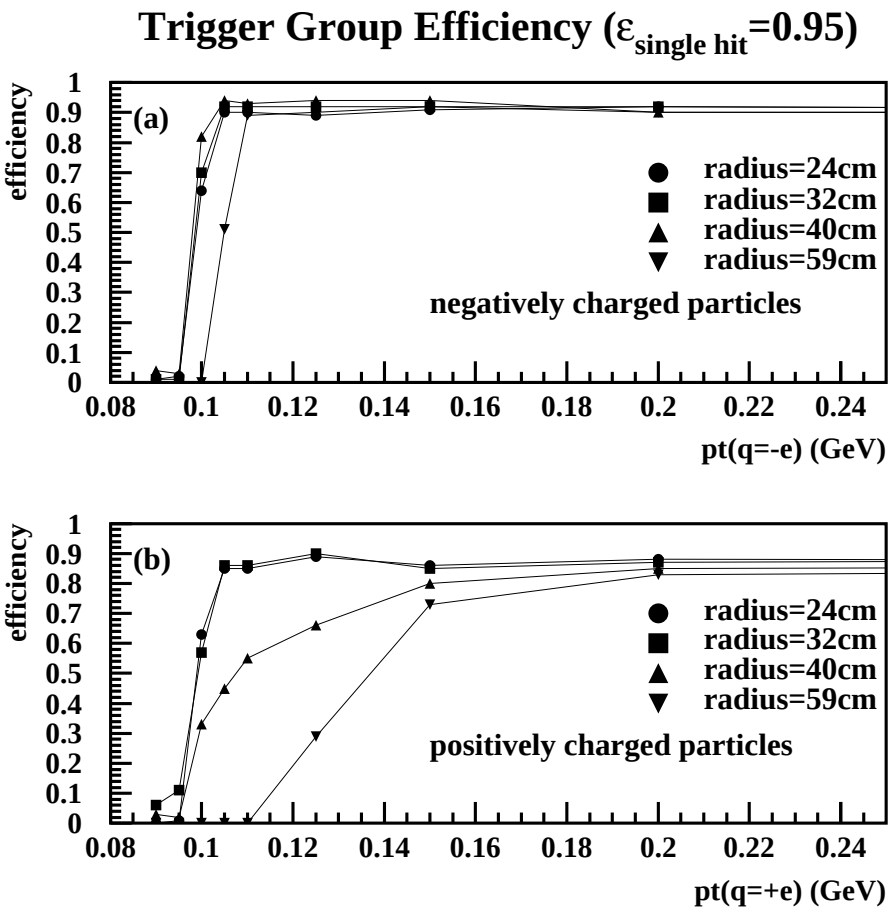

Figure 8: Track segment finding efficiency at four different main radii R as a function of the transverse momentum of the track for (a) negatively charged tracks and (b) positively charged tracks.

4.2 Level 2

After L1 Keep some 25 μs are available for refinement of the trigger decision. This time will be used to link identified track segments and compute track parameters. The track parameters will be passed to a central processing stage where global event properties such as momentum or transverse momentum sums, track topologies and multiplicities can be rapidly evaluated and contribute to the L2 trigger decision.

4.3 Level 3

The impact on the overall operating efficiency of the level 3 filtering depends largely on the decision time involved. If L3 decisions can be made within 100 μs, an increase of the L3 reject rate by 100 Hz can be tolerated whilst causing the deadtime to increase by 1%. Beyond 800 μs an L3 Keep decision will be forced and initiates the readout of all components. L3 reject decisions close to the limit of 800 μs hence have little impact on the filtering capabilities and improve the deadtime only through second order effects when the bandwidth of event building into the level 4 filter farm starts to be limiting.

We therefore envisage to have a dedicated processing engine available, which consists of an assembly of commercial processors. It will perform the necessary 4-vector arithmetic on the track parameters to arrive at a decision. The actual L3 trigger decision will then be based on the outcome of the algorithms running in this engine. The algorithms will aim for the earliest reject decision possible using methods of increasing complexity. While sum of momenta, maximum momentum etc. can be quickly evaluated, correlations between two particles (angles, masses) require more time. The computational effort required to determine invariant masses is simply derived from the large number of combinations that have to be tested. Tight selections of candidate tracks, for instance by defining regions of interesting momentum, can significantly reduce the number of combinations. Finally, for instance, identification of a single D^* candidate using the Δm method will be sufficient to retain the event for readout.

Use of a commercial processor system has several advantages. Firstly, the triggering capabilities are limited only by the data available and the processing power, which can readily be increased. Multiple algorithms can be implemented and development proceeds within a well-defined software environment. The considerable potential of this approach will be investigated as part of the ongoing studies.

5 Implementation

5.1 Overview

The Fast Track Trigger is to use the signals from groups of three wires in three layers in CJC 1 and one group in CJC 2 resulting in a total of 150 groups. Such triplets are sufficient to determine track segments and coarse momentum parameters in conjunction with the main vertex. The *track linker* matches the segments belonging to individual tracks and performs a fit at level 2. Invariant masses are evaluated on level 3.

5.2 Transmission of drift chamber signals to FTT

The input analogue signals of the drift chamber are available on the front panel of the FADC cards and are currently used for the existing DC$r\phi$ [5] trigger. “Piggy-back” connector cards will be mounted on the existing DC$r\phi$ daughter cards as illustrated in figure 9 and will pick up and transmit the analogue information from the desired six wire-ends on each FADC card. The signals for the DC$r\phi$ trigger will be preserved. Because of the

differing groups of wires used in CJC 1 and CJC 2 two different versions of this card will be required. In order to minimise the distance over which these analogue signals need to be transmitted the front-end modules will be located in the two presently unused crates in the Central Tracker read-out aisle, where with some rearrangement of existing electronics this distance will be kept below 5-10 metres. The opportunity is taken here of eventually rearranging the wire signals suitable for the segment finding in the latter stage of the L1 processing.

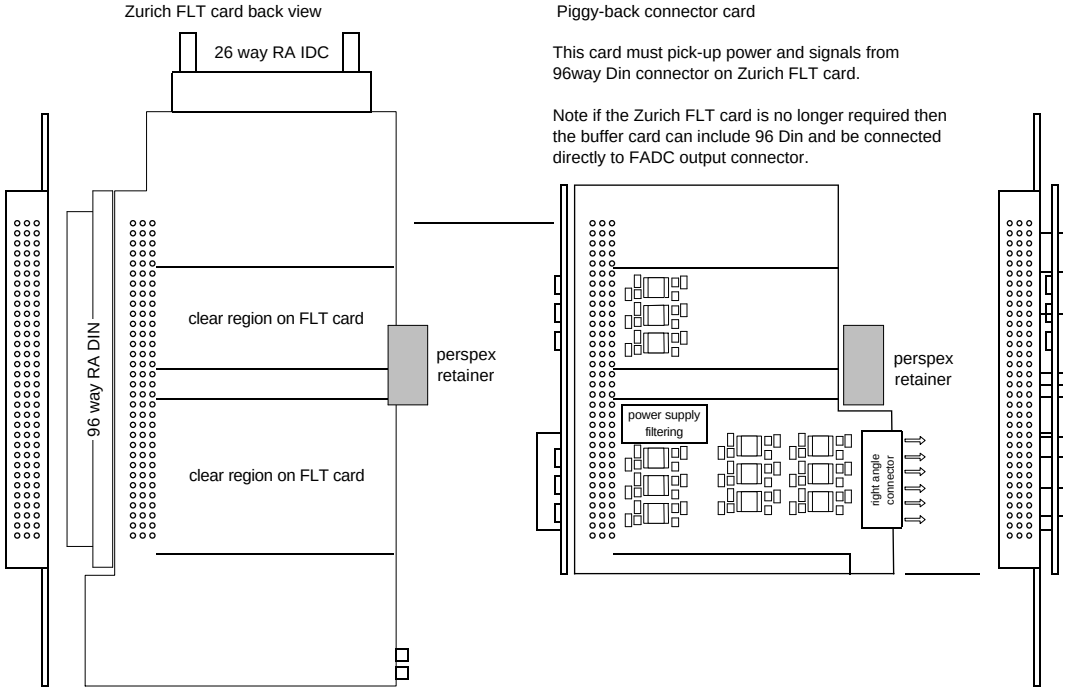

Figure 9: The mounting of the Piggy-back daughter cards onto the adapter cards of the present DC$r\phi$ trigger (Zurich FLT card), which is held in place by a perspex retainer bar. The 96 way connector provides the signals at the front of the FADC card. The add-on board will be placed on the side of the adapter card as can be seen in the right part of the figure.

5.3 First Stage Digitisation

The Front-end module will be a development of the generic MFRTPC [23] card proposed by the Instrumentation Department at CLRC Rutherford Appleton Laboratory. Five such modules, directly integrated onto a larger motherboard (fig. 10), will digitise and process the information from a group of three wires in real time and will effectively consist of two parts, the initial digitisation stage and the segment finding stage. This latter segment finding stage also requires information from the immediately adjacent cells to allow the reconstruction of tracks that cross cell boundaries (fig. 10).

Two possibilities for the first stage digitisation are envisaged; the preference is to digitise the pulses using up to 100 MHz, FADCs followed by a *charge and time* (QT) algorithm implemented on high density *field programmable gate arrays* (FPGA). A potential alternative is to feed the pulses into constant fraction discriminators and extract the hit timing using a TDC (this latter maps more seamlessly onto the FPGA track finding algorithm and could produce the z measurement along the wire direction directly rather than by charge division. It suffers from only having access to the slowed signals designed for the original FADC based read-out, which remains). In either case the information on the z coordinate will be determined by comparing signals from both ends of the wires.

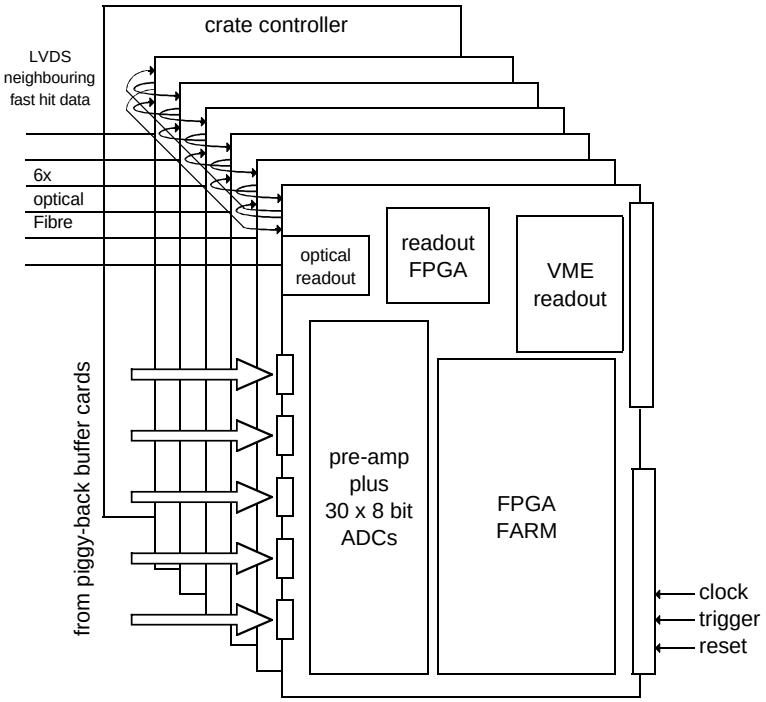

Figure 10: Front-end interconnections

5.4 The QT Analysis

The QT algorithm needs to be fully implemented on FPGA. Since the analysis requires data from both ends of a wire, there will be sufficient input capacity on the FPGA to receive the output of two FADCs. (The final number of FPGAs on a segment finder board will depend on logic integration and price. It will be a matter of careful optimisation.) The algorithm described here [24] is a development of that already used in the H1 drift chamber readout. Such an approach has been followed in detail and it has been shown that the algorithm can be implemented in existing programmable devices and that the timing constraints can be met.

The output from the 100 MHz, 10 bit linear FADCs is fed directly into the FPGA. (We are also studying the use of 8 bit and slower FADCs with the advantage of slightly fewer connections and much reduced cost.) Hit regions are identified for each end of each wire separately, a hit region being defined as two or more samples where the difference in successive samples of the digitised data is above a threshold, followed by two samples where the difference of samples (DOS) is zero or negative. A global hit envelope, for which a single QT hit is produced, is defined from the logical 'OR' of hit regions from both ends of the wire. The time of the first sample of this envelope is also passed directly to the segment finding stage which proceeds in parallel to the rest of the QT analysis, as illustrated in the overview of the QT analysis and segment finding in figure 11.

The accurate time for each end of the wire with a precision of up to 1 ns is derived from the time of the first maximum in DOS within the hit envelope and the ratio of this maximum DOS and the DOS of the immediately preceding sample, using a look-up table. The single time for the hit is the mean of the times from each end of the wire. The charge of the hit is calculated for each end of the wire by integrating over eight digitisations following the start sample with a correction applied to take into account the accurate start time. All calculations are corrected for the pedestal signal level, which is determined from the average of four samples prior to the hit.

In the case of overlapping hits a further correction is applied once the initial hit has been identified by subtracting off a standard pulse tail from the observed data and then using the same techniques for calculating the times

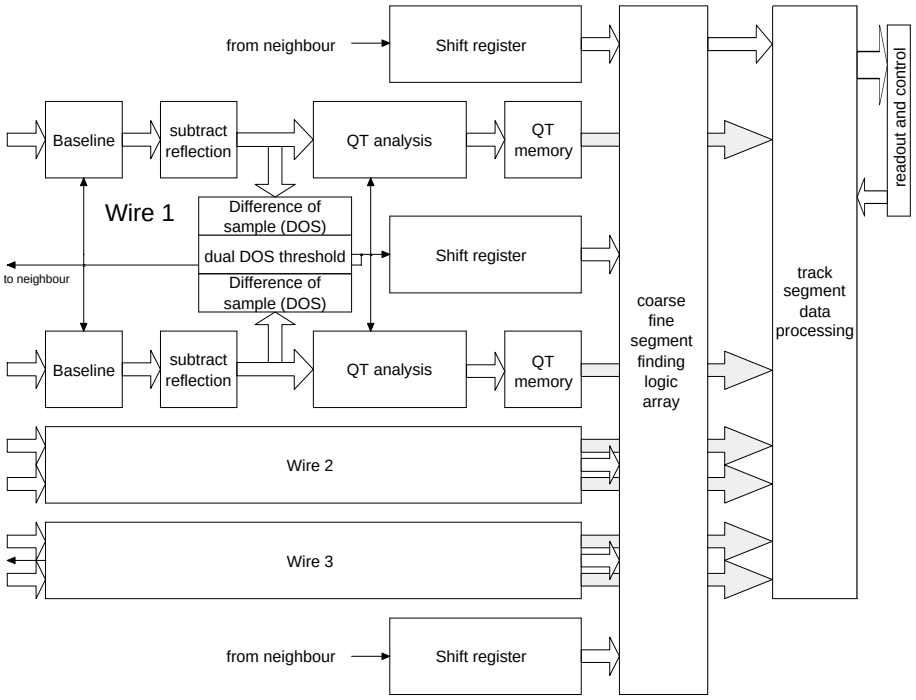

Figure 11: Front-end digitisation and track segment finding on a group of three wires. The logical building blocks of the QT algorithms are indicated for one wire.

and charges as are used for the first or isolated hit which have been described above.

5.5 Hit Processing and Initial Track Recognition

For the segment finding the identified 100 MHz hit data will be fed synchronously into shift registers of 128 bit depth which allow track segments to be recognised by comparing the hits with predefined patterns. In fact, it will be advantageous to insert each hit into several shift registers at the same time. The signals will be fed into two registers to account for the ambiguity as to whether the track passes to the left or right of the sense wire. Further shift registers are required to pass information between cells (fig. 12). This is because the segment finding requires sharing information from the first and last wire in the three wire group with the immediately adjacent cells in the layer in order to pick up tracks which cross a cell boundary, typically at small momentum.

The sets of hit triplets corresponding to acceptable track segments fall into three groups depending on whether the track passes on one side of the cell, passes the wire plane or crosses a cell boundary. While the former case can be generally identified with a track segment even without knowing the bunch crossing of the event, the latter requires knowledge of the bunch crossing as well as of other calibration quantities such as drift velocities (and Lorentz angle) to correctly map the single hit from the adjacent cell into the local drift space. Thus there are two special regions, the wire plane and the separating plane between cells. Since for this proposal we assume that the bunch crossing of the event, the T_0, is known from the L1 Keep, the stored "image" in the shift registers corresponds to the event display of drift chamber information.

The task left is to recognise fairly straight patterns compatible with tracks from the vertex and momentum above 100 MeV. For three layers the number of valid patterns is large (of order 10^6). Taking into account the left/right and adjacent cell solution the number increases even more. However, the double hit resolution is intrinsically limited to order 2 mm making it possible to combine, i.e., to *OR* four or more adjacent time slices, for initial coarse pattern match. In a two stage processes we plan to reduce the a priori 7-bit address

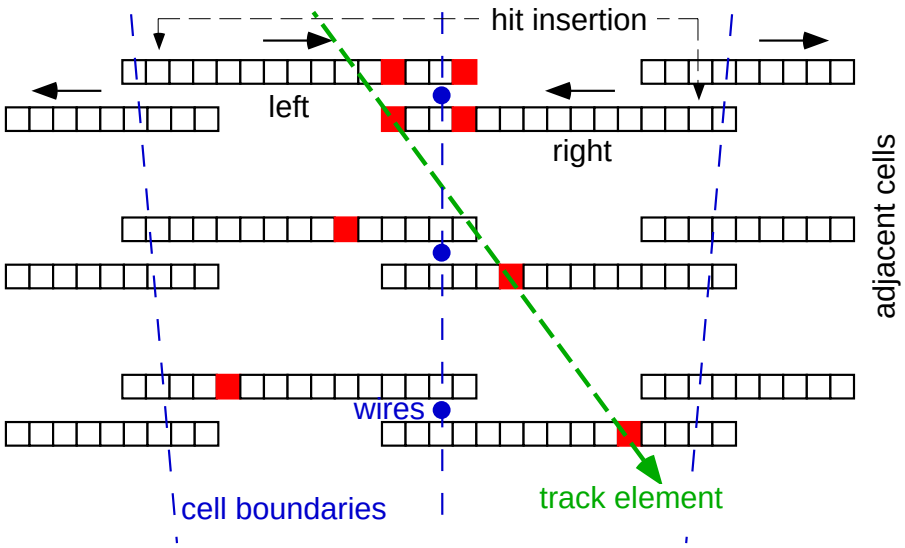

Figure 12: Sketch of the shift registers for the segment finding logic using three adjacent wire planes. The entries in the shift registers corresponding to the left and right drift space solutions are indicated as is the treatment of the adjacent cells. The insertion points are optimised time offsets for each layer. The track indicated crosses the wire plane.

in each shift register to an effective 5-bit address. The resulting 5 bit addresses from each of the three layers could be combined to 15 bits, which could be tested against a look-up-table of valid coarse patterns. Instead of a simple yes/no decision, the look-up table contains the pointer to another table, where after re-activation of the truncated address bits, the validity of the fine pattern can be interrogated. A final look-up into a table with calibrated $1/p_t$ and ϕ values will serve to provide the track parameters in global coordinates. The calibration parameters will have to be updated whenever the operating conditions of the chamber changes, typically on a once per day basis.

Note that this approach entails some detailed book-keeping. The z-coordinates of the hits will have to be registered and the index for accessing the information has to be maintained. Likewise, the nested look-ups will require that proper track is kept of all other ancillary information.

A digital signal processor (DSP) is a natural choice for pattern processing as long as sufficient time is available to treat all information strictly sequentially. A slightly more challenging solution is suggested by the availability of high density logic devices with internal memory. Some of the new devices can be programmed as *content-addressable-memory* (CAM), which can be employed for a high speed pattern match. A natural implementation of the logic required for this step is, e.g. provided by the new Altera devices [25] which not only implement CAMs at high speed but also support LVDS [26] connections to the neighbours on-chip.

5.6 Resolution of ϕ and $1/p_t$

The parameters of the track segments are essentially determined by the resolution on the slope of the 3-wire group elements in conjunction with the vertex constraint ($1/p_t \propto 2 \sin \phi_{\mathrm{slope}}/r$). The expected resolutions on $1/p_t$ and ϕ are shown in Fig. 13. They have been determined from an analysis of H1 data, emulating the trigger response to the available drift chamber data from the complete readout.

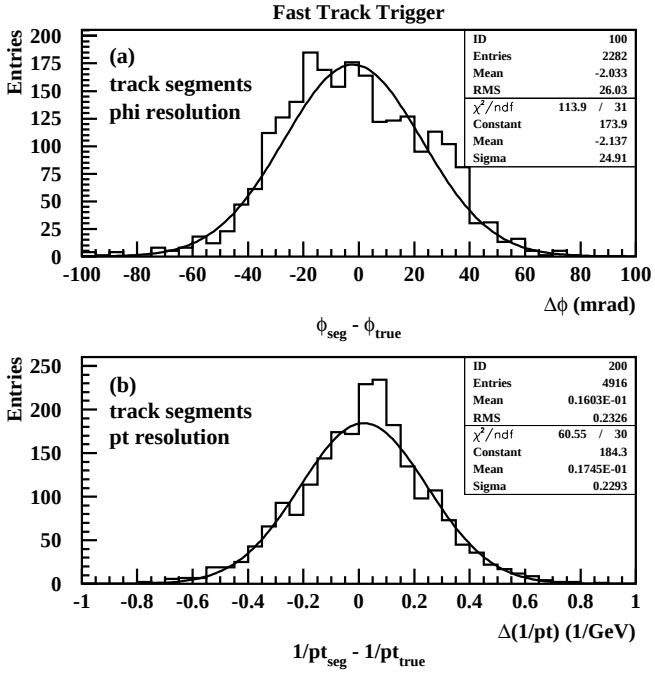

Figure 13: The ϕ (a) and $1/p_t$ (b) resolution of the track segments from $D^* \to K\pi\pi$ candidates selected from data taken in 1997. While the ϕ-resolution is fairly independent of the choice of radial group of wires, the $1/p_t$ resolution improves with R, the radius of the group, due to the longer lever arm.

The reconstructed $1/p_t$ and ϕ values are finally merged with the z-information obtained from the mean z-position of the 3 hits. The resulting $1/p_t$, ϕ and z vector can be represented by a 32-bit word. To better constrain the vertex position along the beam line we plan to use the peak position of the so called zvtx-histogram as an estimator of the z-position [2] of the ep interaction. This number will only be available after L1.

5.7 Transfer of Track Segment Data

For global linking the track segment data have to be shipped to the central crate of the *L2 Track Linker*. Care has to be taken to balance the output loads of 150 track segment finders, of which 3 are associated with each of the 30 azimuthal cells of CJC 1 while one group in CJC 2 necessitates 60 outputs. By grouping 5 non-adjacent cells of CJC 1 and their corresponding 10 neighbour cells of CJC 2, at least six (twelve) logical links to the L2 Track Linker will be necessary to balance the load. We plan to run 30 links of 2 GBit/s to the L2 track linker. For such a configuration the load for typical D^* events is shown in figure 14.

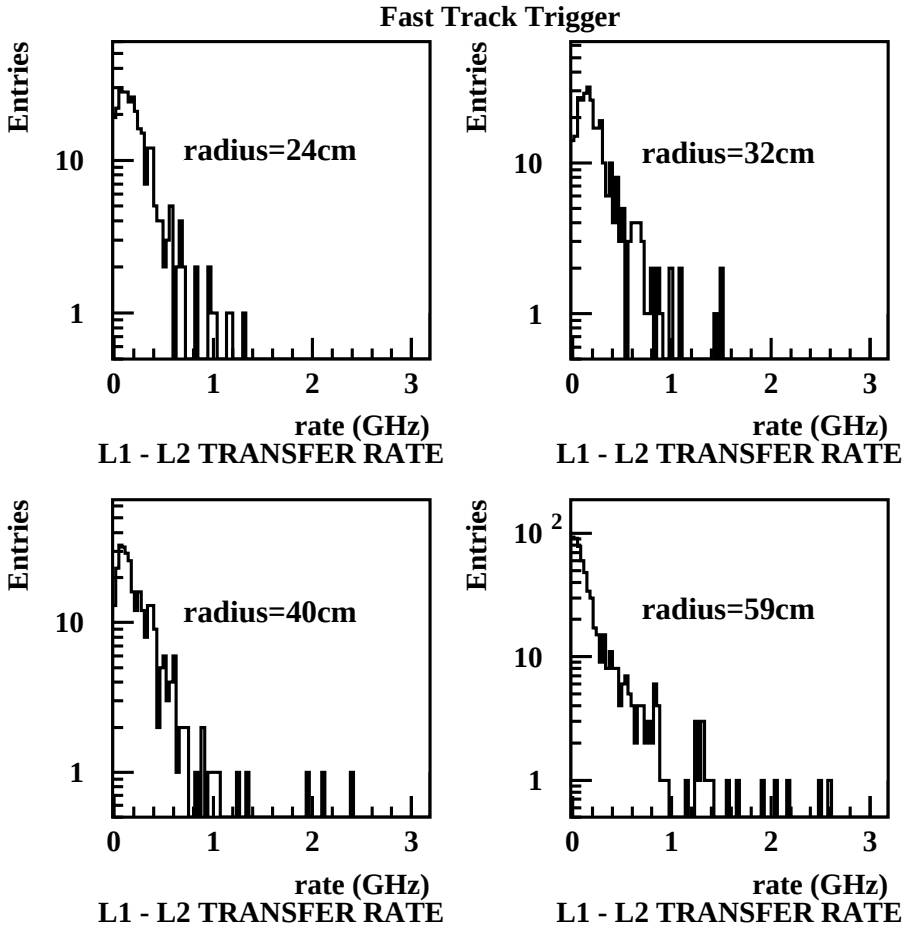

Figure 14: The required transfer rate for segment data in D^* events distinguished according to radial group.

5.8 L2 Track Linker

The task of the L2 Track Linker [27] is to combine track segments of up to four radial groups, derive the best estimate of the track parameters and to reject randomly found track segments of single groups. Real tracks will logically be identified as a cluster of up to four entries in a (virtual) $1/p_t - \phi$ scatter plot.

This task will be accomplished by 4 identical boards equipped with four processor units (L2PU) each. Each of the 4 L2PU receives 8 physical serial data streams from the front-end system. The 32 bit data for each track segment are buffered for each link in a 32 bit wide first-in-first-out buffer (FIFO), chained into one common data stream for transfer to the other cards, thus making all data available for all L2PU. The bandwidth of the installed link allows the transfer of up to 100 track segments per trigger group in 2 μs. The track segment data will be stored in pages of a memory (SRAM), indexed by angle ϕ with granularity 128. This angle can be measured with good resolution for all layers and thus incorrect grouping is not expected to be a problem. Counters associated with each of the 128 pages keep track of the entries.

Load sharing between the 16 L2PU proceeds according to a fixed scheme, where one L2PU deals with a predefined number of up to 32 track segments so that the distribution over several L2PU is known in advance from the values of the counters and does not require further "handshake". Hence, all L2PU will only be invoked in very high multiplicity events. The L2PU operate independently.

The linking of matching track segment data proceeds with the help of *content-addressable-memories* CAMs. Initially a 128 word CAM is allocated to each of the 4 radial groups. The FIFO data are loaded sequentially as patterns in the associated CAM and mirrored to the SRAM memory. "*Don't care*-bits" in the subsequent pattern match restrict the comparisons to the relevant $1/p_t$- and ϕ-bits of the 32 bit track segment word. The pattern match, i.e. addressing the contents, involves a retransmission of all track segments from the SRAM. The 4 distinct CAMs are now treated as an ensemble returning a match condition whenever at least two logical CAM groups indicate equivalent track parameters. On success a list of track segments is generated provided there is no veto condition indicated by a second so called *dirty* CAM. The dirty CAM is filled with the data value of whatever has been detected as a valid match before. The processing steps are illustrated in figure 15 and proceed under the control of the hardware search logic. The steps are repeated until the associated range of the SRAM has been tested. In order to avoid the typical edge effects in such a cluster search we plan to use 4 overlapping sliding windows for the track segment tests.

The scheme is envisaged to be implemented using high density programmable devices. (A very attractive solution is provided by the Altera 20KE PLD [25], of which a single chip would be sufficient for the board. 20 so called embedded system blocks (ESB) would be configured for the 4×128 word deep CAM and its control logic). The algorithm takes about 1 μs for loading of the CAMs and 6 μs for the search.The timing is detailed in table 3.

Process	**time [μs]**
read data from track segment finder	1
distribute data to all L2PU's and load CAMs	2
dynamic load balancing (counters)	1
Search including using 4 sliding windows	6
optimise track parameter values (DSP)	8
distribute track parameters and calculate sums	2
communicate result to L3	1
total	21

Table 3: Performance of the L2PUs. Note that several actions can be interleaved.

The valid output segments are presented to a DSP for proper analysis. The track vectors are first optimised

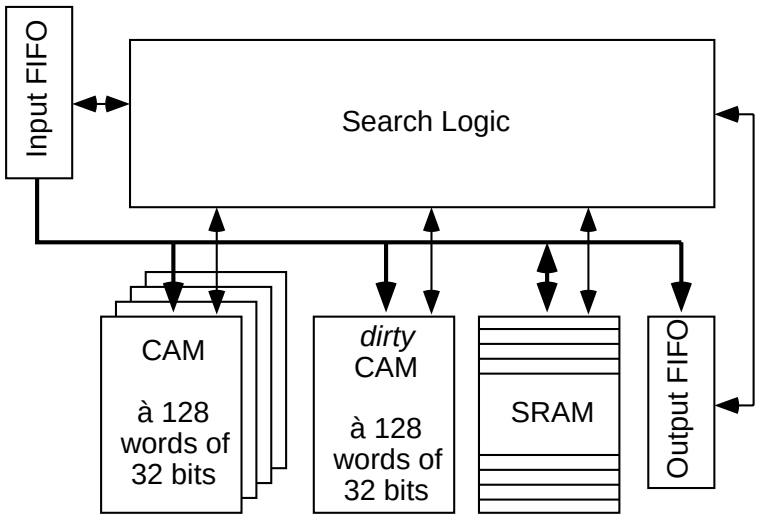

Figure 15: Essential elements of the track linking at level 2 consisting of the 4 fold CAM for the radial groups, the SRAM to store valid track segments organised in ϕ pages, the *dirty* CAM to mark used, valid combinations and the output buffer. The track fitting is not shown.

in the $r\phi$-plane and then in rz. Processing time of the $r\phi$-fit [28] depends on track multiplicity of the event and can be accomplished in a few μs, as has been already shown in a test implementation on a standard RISC work station. A DSP provides sufficient room for code optimisation. It proceeds concurrently with the track segment linking. In parallel, global event quantities such as $\sum p_t$, $|\sum \vec{p}|$, n_{tracks}, or topological properties such as back-to-back tracks, are calculated for the L2-Keep trigger decision. Trigger decisions generated can then be transmitted to the central L2 logic [29], where spare capacity for new inputs is already provided.

5.9 Analysis at Level 3

The L3 trigger readout of the momentum vectors of the four L2 Track Linker modules will proceed inside the same crate. It can be performed over the backplane VME bus to the L3 processing unit. This “trigger engine” will take the form of a set of commercial processors running appropriate trigger algorithms. This approach is scalable and offers an easy upgrade path should the need arise. Furthermore, there exists within H1 significant experience in the use of such processors.

The L3 trigger algorithms will perform the combinatorial 4-vector calculations necessary to select channels of interest. Suitable algorithms and their mapping onto the hardware are under investigation; the processing may be distributed across several modules or several algorithms run in parallel, as appropriate. The output of each calculation will be a Boolean decision; these will be collected by a simple custom module operating in the same crate. Straightforward extension of the existing central L3 logic will be necessary to accommodate the decisions generated by this system.

6 Miscellaneous

6.1 Compatibility with Existing System

The new system will maintain full compatibility with the existing drift chamber readout system. The only change affects the front-end output of the FADC board to the DC$r\phi$ trigger, which should be transparent.

Some minor rearrangement of cables may be necessary to accommodate the small amount of extra rack space required in the tracker aisle of the electronics "rucksack" of H1.

The new system must also provide readout of analysed track segments, momenta and L3 results. All of this information is available in the crate of the L2 Track Linker, which simplifies the task. At this time it has not been clarified whether the produced data will be attached to the readout of the tracker or trigger branch for the central data acquisition (CDAQ) [30]. None of these implementations represents a major obstacle.

6.2 Commissioning the FTT

Commissioning of the FTT will require configuration of all boards from a stand-alone work station. The trigger response during running can be read out without it initially affecting acceptance of events. It will thus be possible to monitor the logic chain in detail, which will have been debugged by presenting test vectors to the logic at all relevant levels. This readback facility will also provide the necessary cross check of the proper loading of calibration constants.

7 Time Schedule

The time schedule is clearly defined by the long HERA upgrade shutdown planned for 2000/2001. During this shutdown we will install the adapters at the output of the FADC boards.

We aim at a full installation of the trigger for the startup after the long shutdown. In order to reach these targets we currently plan to proceed as indicated in Table 4. Note that the largest activities are related to the configuration of the FPGAs, for which detailed simulation tools will be available.

L1:		
	design and	
	specification of interfaces	Oct. 1999
	FADC output adapter prototype	May 2000
	series production of adapter	Oct. 2000
	Analogue Front-end prototype	Oct. 2000
	start of series production	Oct. 2000
	commissioning	Mar 2001
L2:		
	design and	
	specification of interfaces	Oct. 1999
	prototype	June 2000
	series production	Oct. 2000
	commissioning	Mar. 2001
L3:		
	concept	Oct. 1999
	algorithms	Oct. 2000
	commissioning	Mar. 2001
	startup of Fast Track Trigger	mid 2001

Table 4: Tentative time schedule for design and installation of the Fast Track Trigger.

8 Responsibilities

Presently collaborators at Birmingham, DESY, Dortmund, ETH Zurich and RAL are involved in the studies. The sharing of responsibilities is indicated in table 5, although it is understood that with the decision on a single type of FPGA there will be considerable exchange of ideas and expertise throughout the project.

Institute	Interest
RAL	Front-end
B'ham/DESY/Dort./RAL	L1 track segment finding
ETHZ and SCS	L2 Track Linker
Dort. and N.N.	L3 computing engine

Table 5: Sharing of responsibilities among the interested institutes.

Apart from the front-end, where printed circuit boards have to be produced in large quantities, the open architecture of the proposed system affords a natural distribution of tasks over several collaborating institutes. Considerable interest to participate has been expressed by other physicists and engineers inside H1.

9 Costs

The cost of the upgrade is driven by the large number of channels at the front-end. Each of the 450 wires has to be equipped with advanced electronics. A rough estimate of the required circuit (table 6) results in $\approx$585 kDM for the front-end digitisation and primary track segment analysis including the required connectivity to distribute the information.

Front-end cost per wire:	
Item	Cost [DM]
DC$r\phi$ adapter cards	150
Connectors for analog signals	70
FADC	150
FPGA and CAM	800
RAM	30
Rest (line drivers, connectivity,...)	100
Total	1300

Table 6: The estimated cost per wire for hit digitisation and track segment finding.

Note that there is considerable uncertainty in the costs of the FPGA and CAMs. The most attractive solution is that of a very high density FPGA implementing at the same time the CAM. It is not clear whether the device that is currently being introduced [31] will be sufficient or whether the device with twice the capacity announced for later this year will be required. For components very close to market introduction, prices usually run high. We expect this to change because other vendors start to introduce products of similar density [32]. With the quoted cost of ref [31] the price would come down to $\approx$400 kDM.

In addition we have to foresee individual boards for central clock and control signal distribution. Readout links between crates have to be provided for which the PVIC development [33] seems to be an interesting option. These boards will add another $\approx$50 kDM.

The hardware cost of the 4 L2 Track Linker boards is modest. Components add up to $\approx$100 kDM. In addition

1000 kDM will be incurred for the four man-years of development time necessary at the SCS company in Zurich. We plan to reduce these costs by providing skilled manpower to the company of order 1-2 man years equivalent.

The L3 processing will probably depend on a single dedicated processing engine at an estimated price of 50 kDM.

With contingency of ≈20% added the entire project will run at an estimated price of 950 kDM (1600 kDM≈ 950 kDM+ 1000 kDM* 2.5 a/4 a) without (with) labour (table 7).

Overall Project Cost:		
Item	Cost [kDM]	External labour [kDM]
L1 digitisation and track segment finding	585	
Readout interconnections	50	
L2 Track Linker hardware	100	1000
L3 processing	50	
Total	785	1000

Table 7: The overall cost for hardware and external labour.

Prior to demonstration of feasibility we have not attempted to find a complete financing scheme. A large amount (250 kDM) has been set aside from BMBF funds which hopefully can be expanded to a total of 500 kDM. DESY and UK collaborators are encouraged to find support from their home institutes at the level of 250 kDM each, while ETHZ may be able to cooperate directly with the ETH affiliated SCS company.

References

[1] I. Abt, et al, Nucl. Instr. Meth. **A386** (1997) 310 and 348.

[2] M. Cuje et al., *H1 High Luminosity Upgrade, CIP and Level 1 Vertex Trigger*, Proposal submitted to the Physics Research Committee, PRC 98-02.

[3] A. Campbell, et al, *Proposal to Merge Level-4 and Level-5 Systems of the H1 Experiment*, Proposal submitted to the Physics Research Committee, H1-Note H1-12/98-588.

[4] W. Zimmermann et al., *A 16 channel VME flash ADC system (F1001-FADC)*, H1 Internal Report, DESY, Hamburg (1989), unpublished; manufacturer: Struck, Tangstedt, Germany.

[5] T. Wolff et al., *A Drift Chamber Track Finder for the first Level Trigger of the H1 Experiment*, Nucl. Instrum. Meth. **A323** (1992) 537-541

[6] H.-C. Schultz-Coulon, et al, *A general scheme for optimization of trigger rates in an experiment with limited bandwidth*, Nuclear Science Symposium IEEE 1998, Toronto, 8-14 November, 1998

[7] Proceedings of the Workshop *Future Physics at HERA*, ed. G. Ingelman, A. de Roeck, R. Klanner, 1996, available from
http://www.desy.de/∼heraws96.

[8] *The HERA Luminosity Upgrade*, ed. U. Schneekloth, DESY HERA **98-05**, 1998.

[9] H1 Collaboration, C. Adloff et al., Nucl. Phys. **B545** (1999) 21-44

[10] H1 Collaboration, Conf. Paper 558, 29th Intern. Conf. on HEP, Vancouver, Canada (1998).

[11] H1 Collaboration, Conf. Paper 575, 29th Intern. Conf. on HEP, Vancouver, Canada (1998).

[12] H1 Collaboration, C. Adloff et al., DESY **99-010**, submitted to Eur. Phys. J.

[13] H1 Collaboration, C. Adloff et al., DESY **99-026**, submitted to Eur. Phys. J.

[14] A. Mueller, W. Tang, Phys. Lett. **B284** (1992) 123.

[15] H1 Collaboration, paper 274 at Int. Europhys. Conf. on HEP, Jerusalem, August 1997.

[16] H1 Collaboration, Conf. Paper 574, 29th Intern. Conf. on HEP, Vancouver, Canada (1998).

[17] L. Frankfurt, M. McDermott, M. Strikman, JHEP **9902** (1999) 002.

[18] C. Adloff et al., Nucl. Phys. **B485** (1997) 3.

[19] C. Adloff et al., Eur. Phys. J. **C5** (1998) 575.

[20] G. Ingelman, J. Rathsman, G. Schuler, Comp. Phys. Commun. **101** (1997) 135.

[21] T. Carli et al., *Proposal to Upgrade the LAr Calorimeter Trigger: The Jet Trigger*, Proposal submitted to the Physics Research Committee, PRC 99-02, H1-Note H1-01/99-560

[22] W.J. Haynes, *H1 Data Acquisition 2000*, H1 Internal Document, July 1997.

[23] S.A.Baird, *The MFRTPC Project*, Proposal Rutherford Laboratory, UK.

[24] D.P.C. Sankey, *The Proposed QT Algorithm for the Fast Track Trigger*, Internal Project Document.

[25] *Altera*,
http://www.altera.com

[26] *LVDS*, National Semiconductor,
http://www.national.com/catalog/AnalogInterface_LVDSCircuits.html

[27] This proposal has been drafted in close collaboration with SuperComputing Systems, Zurich, Switzerland
http://www.scs.ch

[28] V. Karimäki, Nucl. Instr. Meth. **A305** (1991) 187.

[29] T. Nicholls, et al., *Concept, Design and Performance of the Second Level Triggers of the H1 Detector*, IEEE Trans, Nucl. Sci. **45** (1998) 810.

[30] W.J. Haynes, *Bus-based Architectures in the H1 Data Acquisition System*, Presentation to the International Conference “Open Bus Systems”, Zürich, October 1992.

[31] Altera announce in a press release of April 16, 1999 the shipment of the base version of the EP20K400 chip and forecast an end 1999 volume price of $\approx$\$ 200,
http://www.altera.com/html/new/pressrel/pr_apex-ship.html

[32] XILINX
http://www.xilinx.com/products/virtex.htm

[33] *PVIC, The PCI Vertical Interconnection*, Creative Electronic Systems,
http://www.ces.ch/Products/Connexions/PVICFamily/PVIC.html